Periodic Macroporous Nanocrystalline Antimony-Doped Tin Oxide Electrode

Eric Arsenault, Navid Soheilnia, and Geoffrey A. Ozin*

Materials Chemistry and Nanochemistry Research Group, Centre for Inorganic and Polymeric Materials, Department of Chemistry, University of Toronto, 80 St. George Street, Toronto, Ontario M5S 3H6, Canada

ABSTRACT Optically transparent and electrically conductive electrodes are ubiquitous in the myriad world of devices. They are an indispensable component of solar and photoelectrochemical cells, organic and polymer light emitting diodes, lasers, displays, electrochromic windows, photodetectors, and chemical sensors. The majority of the electrodes in such devices are made of large electronic band-gap doped metal oxides fashioned as a dense low-surface-area film deposited on a glass substrate. Typical transparent conducting oxide materials include indium-, fluorine-, or antimony-doped tin oxides. Herein we introduce for the first time a transparent conductive periodic macroporous electrode that has been self-assembled from 6 nm nanocrystalline antimony-doped tin oxide with high thermal stability, optimized electrical conductivity, and high quality photonic crystal properties, and present an electrochemically actuated optical light switch built from this electrode, whose operation is predicated on its unique combination of electrical, optical, and photonic properties. The ability of this macroporous electrode to host active functional materials like dyes, polymers, nanocrystals, and nanowires provides new opportunities to create devices with improved performance enabled by the large area, spatially accessible and electroactive internal surface.

KEYWORDS: transparent conducting oxide · macroporous electrode · electrooptical switch · antimony-doped tin oxide · inverse opal

Transparent conducting oxides (TCOs) are the cornerstone of optoelectronic devices, allowing light to transmit with minimal losses while simultaneously transporting charge. Together with their low electrical resistivity and high thermal stability these properties render TCOs ideally suited as electrodes to meet a multitude of optoelectronic and photoelectrochemical device requirements. To exploit the full potential of TCOs as electrode materials for various device applications, besides dense planar forms of the material, it is also necessary to find a means to make them porous at length scales traversing the microscopic (<2 nm) through the mesoscopic (2−50 nm) to the macroscopic (>50 nm with 1, 2, or 3 dimensionality).[1] Nothing currently exists in the open or patent literature on any kind of TCO fashioned with arrays of macropores, either periodically or aperiodically arranged.

Structuring TCO electrodes into novel architectures over different length scales and dimensionality is emerging as a powerful way to boost current densities and shorten electron transport distances for a range of device applications.[2−5] To date, structured electrode materials have been produced using bottom-up techniques such as electroplating,[6] dealloying,[7] and surfactant or colloidal crystal templating.[8,9] Periodic macroporous electrodes made by template replication of opals have been described for carbon and silicon for use as anodes in lithium ion batteries[5,10] and metallic inverse opals for applications in electrocatalysis.[11] The preparation of (electro)chemically stable macroporous TCO has however remained elusive due to materials synthesis challenges associated with the doping requirements to achieve desired electrical and optical properties. In addition, maintaining structural integrity has remained a challenge due to adverse mechanical effects associated with chemically induced shrinkage during formation.

We have managed to surmount these obstacles thanks to recent progress in the synthesis of colloidally stable TCO nanocrystals.[12] Described herein we present the synthesis details, structure determination, properties measurements, and demonstration of electrode function for the first example of a periodic macroporous TCO film. The synergism of optical, electrical, and structural properties of the material is exploited to create a novel electrochemically actuated optical switch, which relies on the reversible electrodeposition and electrodissolution of bismuth metal *within* the macropores to modify in a predetermined cyclic manner the photonic properties of the material from light diffracting to light absorbing in the visible wavelength range. This proof-of-concept demonstration highlights the ability of a periodic macroporous TCO light scale material to host another material, while exploiting its electrical, optical, and photonic properties to perform a specific function. This capability is impossible for either periodic microporous or mesoporous TCO length scales due to their inability to diffract visible light. This key point is amplified upon in what follows.

* Address correspondence to gozin@chem.utoronto.ca.

Received for review January 5, 2011 and accepted March 10, 2011.

Published online March 10, 2011
10.1021/nn2000492

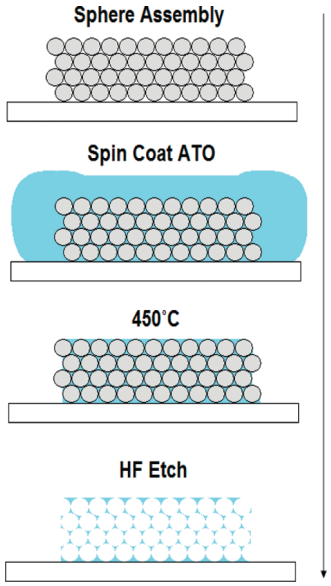

Figure 1. Self-assembly steps for i-ATO-o. Spheres are first assembled *via* EISA. The calcined opal is then infiltrated and spin-coated multiple times with ATO nanocrystals as well as ATO sol. The film is then heated and etched with 1% HF.

Why is the control of pore size and crystalline porosity in TCO film important? First of all, in contradistinction to known periodic mesoporous TCO film, a periodic macroporous TCO film can function as a photonic crystal displaying optical diffraction tunability and slowing of light, enabling it to be utilized for example as an optoelectronic chemical sensor or to enhance photon harvesting in solar cells. Second, the large pores of this TCO material allow efficient mass fluid flow through the open structure permitting their contact with the large internal surface of the electrode. Furthermore, a macroporous TCO has the ability to *host* another material within the voids including various nanoparticles for solar cell, light emitting diode, and sensor applications. Because of the attributes of this genre of TCO, in this study it has proven possible for a periodic macroporous TCO film to be used as a reversible electrochemically actuated photonic crystal optical switch, illustrating thereby its distinction from all other forms of dense or porous TCOs.

The most commonly used TCOs for electrodes are fluorine- and indium-doped tin oxide, denoted FTO and ITO, respectively. TCOs can be produced in a variety of ways, including spray pyrolysis,[13] sol−gel techniques,[14] chemical vapor deposition,[15] and chemical bath deposition.[16] In this study, 6 nm ncATO was used as a building block for synthesizing an inverse nanocrystalline antimony-doped tin oxide opal denoted i-ncATO-o, enabling a straightforward and scalable method to create a transparent conducting periodic macroporous film able to function as an electrode for the operation of an prototypical electrochemical redox reaction and demonstration of a proof-of-concept electro-optical light valve. It is important to note that compared to indium tin oxide ITO, the antimony analogue ATO is a more thermally stable and lower cost material due to the low earth abundance and thus high price of indium.

RESULTS

The assembly of the periodic macroporous TCO framework is outlined in Figure 1. In brief, a silica opal film was grown by evaporation induced self-assembly and infiltrated with ncATO, which was synthesized according to a modified literature preparation.[12] The particle size of as-synthesized ncATO was shown to be 6 nm by dynamic light scattering (DLS), 5−7 nm by scanning electron microscopy (SEM), and 5 nm by powder X-ray diffraction (PXRD), (Figures S3−S5, Supporting Information). The very small size of ncATO was crucial for its controlled infiltration into the void spaces of the silica opal lattice. The as-synthesized ncATO solution was spin-coated into the silica opal film, resulting in an infiltrated opal template with little to no excess nanoparticles covering the opal template. The resulting ncATO-SiO_2-o film was then heated to 450 °C in air to provide mechanical strength to the ncATO framework. The effectiveness of the infiltration was judged from the optically determined volume filling fraction determined from the Bragg−Snell equation (Figure 2b). The infiltration of ATO within the opal structure reduces the refractive index contrast between the spheres and the surrounding matrix, resulting in a red shift of the Bragg peak as well as a decrease in reflectivity.[17] At this stage of the synthesis, etching of SiO_2 spheres resulted in a collapsed structure and thus a method to improve mechanical stability was required. To accomplish this goal, ATO sol was infiltrated into the voids between ncATO in the ncATO-SiO_2-o film and thermally treated to yield an ATO composite with improved structural stability and higher conductivity.[14] The silica spheres were then etched with 1% HF. The filling fraction of this mechanically enhanced i-ncATO-o was calculated to be 65% percent as determined by the wavelength of the optical Bragg reflection.

The results of PXRD indicate a cassiterite structure (SnO_2) for both ncATO and ATO sol (Figure 3). Samples were prepared by spin coating solutions of ATO nanocrystals and ATO sol on a silicon wafer and calcining them at 450 °C for 2 h before measurement. PXRD shows a higher crystallinity in ncATO compared to ATO sol consistent with the higher conductivity observed in ncATO samples, presented below. In addition, XPS was performed on the ATO nanocrystals with an antimony doping of 6.6 atom % compared to an antimony doping of 3.2 atom % in ATO sol which also plays a significant role in the conductivity of these materials (Figure S6, Supporting Information).[12]

Conductivity and porosity measurements were performed on the ATO nc, ATO sol, and ATO composite films. Films of pure ATO nanocrystals and sol reveal

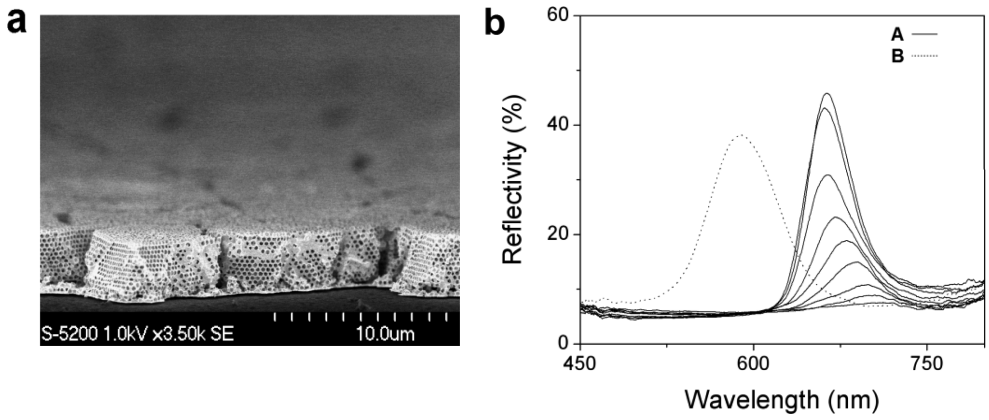

Figure 2. Structure and optical reflectivity spectra of i-ncATO-o films. (a) SEM image of i-ncATO-o film. (b) Optical reflectivity spectra of the silica opal template A, showing the progression of the ncATO infiltration into the silica opal template, depicted by the decrease in intensity and red shift of the Bragg stopband and B, after silica opal template removal resulting in the i-ATO-o film shown in panel a.

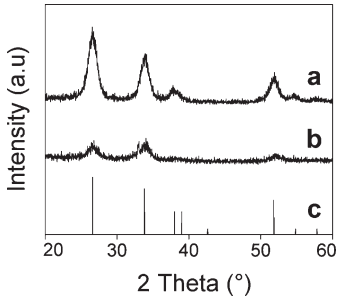

Figure 3. Crystal structure of the ATO materials. (a) PXRD data of ATO nanocrystals, (b) ATO sol, and (c) reference PXRD reflections diagnostic of the tin dioxide cassiterite structure.

that the nanocrystals are significantly more conductive and porous than the ATO sol (Figure 4). The resistance of spin coated ATO films were measured by the four-probe Van-der Pauw method, a well established technique for measuring the resistivity of arbitrary shape samples.[18] Results indicate that ncATO films with ATO sol post infiltration (termed ATO composite) has the lowest resistance. Ellipsometric porosimetry measurements confirm that the porosity of the i-ncATO-o film is greatly reduced by ATO sol infiltration. We attribute the low resistance of the ATO composite to consolidation of the grain boundaries between ncATO as well as a decrease in porosity from the infiltration of ATO sol in the void spaces between ncATO in the i-ncATO-o framework, creating percolative charge transport pathways between the nanocrystals, as seen in the image presented in Figure 4.[19−21] It is interesting that with just one treatment of ATO sol, the conductivity and porosity of the film reaches a plateau.

The use of i-ncATO-o as a platform electrode for electrochemistry was investigated by cyclic voltametry using ferrocene as a representative redox shuttle (Figure 5). The redox activity of i-ncATO-o is found to be slightly higher than the pristine ncATO thin film of the same weight produced *via* spin coating. It is believed that the reason for this is due to the higher accessible surface area of the electrode to ferrocene in the i-ncATO-o film compared to ncATO in planar ncATO films.

To demonstrate functionality of the periodic macroporous TCO electrode, a prototype electrochemical photonic crystal switch was constructed whose operation is founded on the reversible electrodeposition of bismuth within the void spaces of the i-ncATO-o electrode to tune its photonic crystal properties. In our demonstration cyclic voltammetry was performed from −2 to +2 V at a scan rate of 20 mV/s (Figure S7, Supporting Information) of a bismuth(III) electrolyte contained within the i-ncATO-o photonic crystal electrode. As a result, the optical Bragg diffraction intensity of i-ncATO-o was dramatically reduced, resulting in a switching from a red reflective state to a black absorbing state. The origin of this change is the absorption of light of the electrodeposited bismuth throughout the visible wavelength range preventing photon penetration into the photonic lattice thereby eliminating the opportunity for Bragg diffraction (Figures S8 and S9, Supporting Information).[22] SEM images after electrodeposition of bismuth showed the metal within and around the macropores of the i-ncATO-o electrode. X-ray photoelectron spectroscopy (XPS) analysis performed on the i-ncATO-o sample before and after electrodeposition of bismuth provides additional evidence for the deposition of bismuth on the i-ncATO-o electrode (Figures S10 and S11, Supporting Information).

In summary, a periodic macroporous transparent conducting oxide, denoted i-ncATO-o, is presented which for the first time offers a unique synergistic combination of optical transparency, electrical conductivity, and photonic crystal properties. Besides the demonstration of a prototype reversible, electrochemically activated light valve for the i-ncATO-o electrode, its large internal surface area and easily accessible network of interconnected macropores makes the i-ncATO electrode

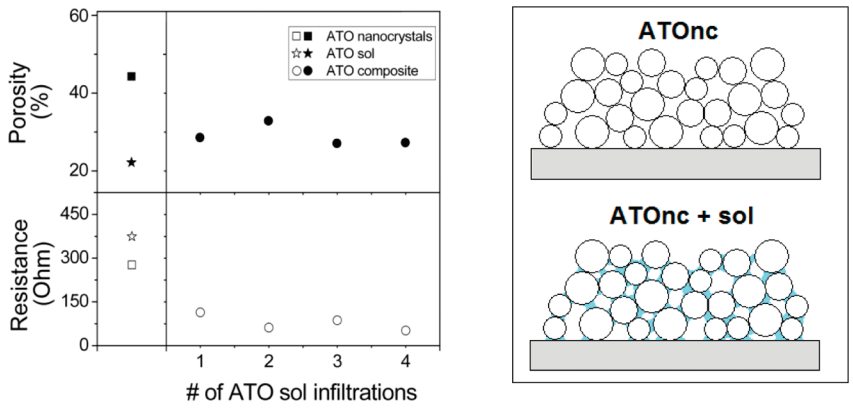

Figure 4. Resistance (four probe) and porosity (ellipsometric porosimetry) measurements of the ATO nanocrystals, sol, and composite materials. The ATO composite materials consist of ATO nanocrystals infiltrated with ATO sol (1−4 infiltrations) by spin coating a solution of sol on the nanocrystal film. The image on the right depicts improved connectivity between ATO nanoparticles resulting in lower porosity, higher conductivity, and better mechanical stability.

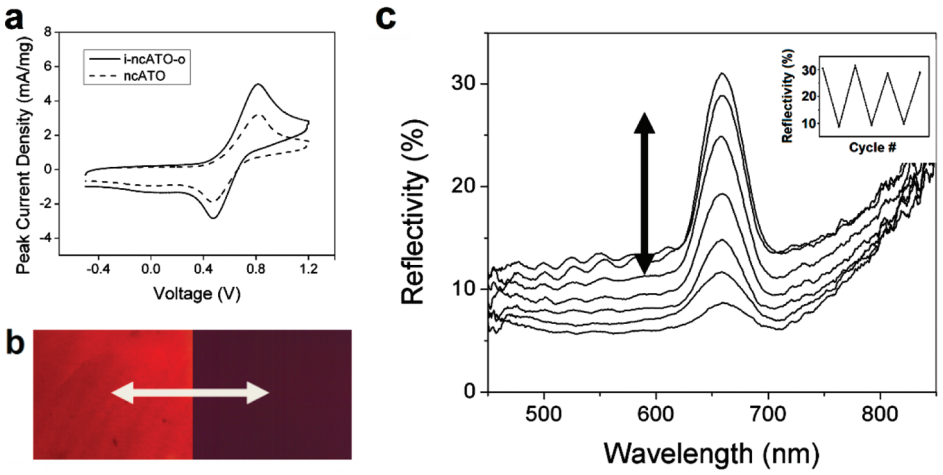

Figure 5. Periodic macroporous transparent oxide i-ncATO-o electrode. (a) Comparison of cyclic voltammograms of ferrocene with i-ncATO-o and ncATO thin film electrodes of the same weight. (b) Optical images of the i-ncATO-o electrode before (left) and after bismuth electrodepsoition (right). (c) Optical reflectivity data obtained during the cyclic electrodeposition of bismuth in the i-ncATO-o photonic crystal electrode, where the insert shows the reversibility of the process.

interesting for the development of a number of enhanced performance photoelectrochemical devices, like dye sensitized solar and water splitting cells, light emitting diodes, and chemical sensors.

EXPERIMENTAL SECTION

All the chemicals for this study were purchased from Sigma-Aldrich Co. without further purifications.

i-ncATO-o Film. The procedure to make the film is as follows: Spheres were grown *via* a modified Stöber method.[23] The as-synthesized spheres were centrifuged and resuspended in ethanol five times and diluted to a 10 wt % solution. An opal film was grown by the evaporation-induced self-assembly (EISA) of silica spheres at 40 °C over 3 days on an FTO substrate. The opal sample was then thermally treated to 450 °C to provide the film with enhanced mechanical stability. ATO nanocrystals and ATO sol were used for infiltration of opal film. These solutions were spin coated above the opal film, followed by heat treatment at 450 °C. The samples were etched in 1% HF overnight to remove the silica sphere template. ncATO did not etch in HF.

ncATO Preparation. A previously published method with modifications was used for synthesis of ATO nanocrystals.[12] A mixture of 0.4010 mmol of $SbCl_3$ and 1.2967 mmol of $SnCl_4$ was slowly added to 20 mL of benzyl alcohol. The mixture then was placed in the oven at 140 °C for 2 h. Nanocrystals separated from the solution were washed with acetone and ethanol several times to separate organic residue from the nanocrystals.

ATO Sol Preparation. ATO sol was prepared in two different vials. A mixed solution of 59.8 mmol $SnCl_2 \cdot 2H_2O$, 50 mL of acetic acid, and 50 mL of ethanol was prepared. The mixture was then stirred for 2 h at 70 °C. A second mixed solution was prepared by adding 2.4 mmol of $SbCl_3$, 25 mL of acetic acid, and 25 mL of ethanol. The mixture was stirred for 2 h at 70 °C. The ATO sol was prepared by adding the two precursor solutions and stirring for another 2 h at 70 °C and aging for 24 h.

Cyclic Voltametry. A 10 mM solution of ferrocene and 0.5 M tetrabutylammonium hexafluorophosphate in acetonitrile was used for cyclic voltametry measurements. Voltage ranges used were −500 mV to 1200 mV at a scan rate of 100 mV/s. Platinum counter and reference electrodes were used. Sample weights were measured using a Mettler TOLEDO MX5 microbalance.

Electrodeposition. Electrodeposition of bismuth was performed on i-ncATO-o films prepared on glass substrates. Electrical contacts to i-ncATO-o film were made using silver paste. The entire film was immersed in an electrolyte solution and placed within a Petri dish under the eyepiece of an optical microscope fitted with a camera and fiber optic microoptical reflectance spectroscopy attachment. Bismuth films were electrodeposited according to literature. A 1 M HCl solution containing 0.02 M $BiCl_3$, 0.5 M LiBr, and 3 mM $CuCl_2$ was electroplated using a BAS epsilon potentiostat in a conventional 3-electrode electrochemical cell using the cyclic voltammetry setting from −2 V to 2 V at a scan rate of 20 mV/s. Counter and reference electrodes were both platinum. Optical spectra were obtained using an Ocean Optics SD2000 fiber optic spectrophotometer along with an optical microscope. SEM images were obtained on a Hitachi HD-2000. Spectroscopic ellipsometry analyses were performed in a Sopra GES-5E ellipsometer at a fixed incidence angle of 70.15° in the range 1.2−3.5 eV. The modeling and regression analyses of the ellipsometric spectra were performed using the software Winelli provided by the manufacturer. Low angle X-ray diffraction patterns were acquired with a Siemens D5000 diffractometer using Cu Kα1 radiation operated at 50 KV and 35 mA with a Kevex solid-state detector. Wide angle X-ray scattering patterns were obtained with a Bruker D8 diffractometer operated at 40 KV and 40 mA.

Acknowledgment. G.A.O. is a Government of Canada Research Chair in Materials Chemistry and Nanochemistry. He is deeply indebted to the Natural Sciences and Engineering Research Council of Canada for Discovery and Solar Network funding of their research. E.D.A. would like to thank the Natural Sciences and Engineering Research Council of Canada for a CGS scholarship. The authors would like to thank Zhuoying Xie and Wendong Wang for technical support and advice.

Supporting Information Available: Additional SEM images and material as described in the text. This material is available free of charge *via* the Internet at http://pubs.acs.org.

REFERENCES AND NOTES

1. Hou, K.; Puzzo, D.; Helander, M. C.; Lo, S. S.; Bonifacio, L. D.; Wang, W.; Lu, Z. -.; Scholes, G. D.; Ozin, G. A. Dye-Anchored Mesoporous Antimony-Doped Tin Oxide Electrochemiluminescence Cell. *Adv. Mater.* **2009,** *21*, 2492–2496.
2. O'Brien, P. G.; Puzzo, D. P.; Chutinan, A.; Bonifacio, L. D.; Ozin, G. A.; Kherani, N. P. Selectively Transparent and Conducting Photonic Crystals. *Adv. Mater.* **2010,** *22*, 611–616.
3. Fan, Z.; Ruebusch, D. J.; Rathore, A. A.; Kapadia, R.; Ergen, O.; Leu, P. W.; Javey, A. Challenges and Prospects of Nanopillar-Based Solar Cells. *Nano Res.* **2009,** *2*, 829–843.
4. Martinson, A. B. F.; Elam, J. W.; Liu, J.; Pellin, M. J.; Marks, T. J.; Hupp, J. T. Radial Electron Collection in Dye-Sensitized Solar Cells. *Nano Lett.* **2008,** *8*, 2862–2866.
5. Esmanski, A.; Ozin, G. A. Silicon Inverse-Opal-Based Macroporous Materials as Negative Electrodes for Lithium Ion Batteries. *Adv. Funct. Mater.* **2009,** *19*, 1999–2010.
6. Soleymani, L.; Fang, Z.; Sargent, E. H.; Kelley, S. O. Programming the Detection Limits of Biosensors through Controlled Nanostructuring. *Nat. Nanotechnol.* **2009,** *4*, 844–848.
7. Erlebacher, J.; Aziz, M. J.; Karma, A.; Dimitrov, N.; Sieradzki, K. Evolution of Nanoporosity in Dealloying. *Nature* **2001,** *410*, 450–453.
8. Yan, H.; Blanford, C. F.; Holland, B. T.; Parent, M.; Smyrl, W. H.; Stein, A. Chemical Synthesis of Periodic Macroporous NiO and Metallic Ni. *Adv. Mater.* **1999,** *11*, 1003–1006.
9. Bartlett, P. N.; Birkin, P. R.; Ghanem, M. A. Electrochemical Deposition of Macroporous Platinum, Palladium and Cobalt Films Using Polystyrene Latex Sphere Templates. *Chem. Commun.* **2000,** 1671–1672.
10. Lee, K. T.; Lytle, J. C.; Ergang, N. S.; Oh, S. M.; Stein, A. Synthesis and Rate Performance of Monolithic Macroporous Carbon Electrodes for Lithium-Ion Secondary Batteries. *Adv. Funct. Mater.* **2005,** *15*, 547–556.
11. Huang, Y.-J.; Lai, C.-H.; Wu, P.-W.; Chen, L.-Y. A Facile Approach to Fabricate Ni Inverse Opals at Controlled Thickness. *Mater. Lett.* **2009,** *63*, 2393–2395.
12. Müller, V.; Rasp, M.; Štefanić, G.; Ba, J.; Günther, S.; Rathousky, J.; Niederberger, M.; Fattakhova-Rohlfing, D. Highly Conducting Nanosized Monodispersed Antimony-Doped Tin Oxide Particles Synthesized *via* Nonaqueous Sol−Gel Procedure. *Chem. Mater.* **2009,** *21*, 5229–5236.
13. Shanthi, E.; Dutta, V.; Banerjee, A.; Chopra, K. L. Electrical and Optical Properties of Undoped and Antimony-Doped Tin Oxide Films. *J. Appl. Phys.* **1980,** *51*, 6243–6251.
14. Terrier, C.; Chatelon, J. P.; Roger, J. A. Electrical and Optical Properties of Sb:SnO_2 Thin Films Obtained by the Sol−Gel Method. *Thin Solid Films* **1997,** *295*, 95–100.
15. Kim, K.-S.; Yoon, S.-Y.; Lee, W.-J.; Ho Kim, K. Surface Morphologies and Electrical Properties of Antimony-Doped Tin Oxide Films Deposited by Plasma-Enhanced Chemical Vapor Deposition. *Surf. Coat. Technol.* **2001,** *138*, 229–236.
16. Luo, W.-H.; Tsai, T.-K.; Yang, J.-C.; Hsieh, W.-M.; Hsu, C.-H.; Fang, J. Enhancement in Conductivity and Transmittance of Zinc Oxide Prepared by Chemical Bath Deposition. *J. Electron. Mater.* **2009,** *38*, 2264–2269.
17. Hatton, B.; Kitaev, V.; Perovic, D.; Ozin, G.; Aizenberg, J. Low-Temperature Synthesis of Nanoscale Silica Multilayers−Atomic Layer Deposition in a Test Tube. *J. Mater. Chem.* **2010,** *20*, 6009–6013.
18. Van der Pauw, L. J. A Method of Measuring Specific Resistivity and Hall Effect of Discs of Arbitrary Shapes. *Philips Res. Rep.* **1958,** *13*, 1–9.
19. Montes, J. M.; Cuevas, F. G.; Cintas, J. Porosity Effect on the Electrical Conductivity of Sintered Powder Compacts. *Appl. Phys. A* **2008,** *92*, 375–380.
20. Riefler, N.; Mädler, L. Structure−Conductivity Relations of Simulated Highly Porous Nanoparticle Aggregate Films. *J. Nanopart. Res.* **2010,** *12*, 853–863.
21. Benkstein, K. D.; Kopidakis, N.; Van, d. L.; Frank, A. J. Influence of the Percolation Network Geometry on Electron Transport in Dye-Sensitized Titanium Dioxide Solar Cells. *J. Phys. Chem. B* **2003,** *107*, 7759–7767.
22. Córdoba De Torresi, S. I.; Carlos, I. A. Optical Characterization of Bismuth Reversible Electrodeposition. *J. Electroanal. Chem.* **1996,** *414*, 11–16.
23. Stöber, W.; Fink, A.; Bohn, E. Controlled Growth of Monodisperse Silica Spheres in the Micron Size Range. *J. Colloid Interface Sci.* **1968,** *26*, 62–69.